Supporting Information

Dual active site-mediated Ir single-atom-doped RuO_2 catalysts for highly efficient and stable water splitting

Zhenhua Tao, Ning Lv, Hongyu Zhao, Xu Luo, Zilan Li, Jun Yu, Lie Chen, Xupo Liu, Shichun Mu

Experimental Details

1.1 Computational Details

The Density functional theory (DFT) calculations were conducted in the Vienna Abinitio Simulation Package (VASP). The electron exchange and correlation energy were treated with the Perdew-Burke-Ernzerhof (PBE) functional within the generalized gradient approximation (GGA)[1,2]. The ion cores-valence electrons interactions were described through the projected augmented wave (PAW) means, and the van der Waals interactions were eliminated with Grimme's method[3]. The simulations were implemented with a plane-wave basis set defined by a kinetic energy cutoff of 400 eV, and a 1×1×1 Monkhorst Pack k-point grid was used to integrate the Brillouin zone[4,5]. The geometry optimization and energy calculation were terminated when the electronic selfconsistent iteration and force reached 10^{-5} eV and 0.02 eV $Å^{-1}$. The theoretical models were built based on the (110) of RuO_2 (PDF#40-1290) and (110) of IrO_2 (PDF 04-006-7402).

The calculation model of Ir single atom doped RuO_2 (Ir_{SA}/RuO_2) was constructed by Replacement of Ru atoms in RuO_2 crystals by Ir atoms (96 O, 47Ru, 1 Ir atoms). A vacuum space as large as 15 Å was used along the c direction to avoid periodic interactions. The k-point sampling was obtained from the Monkhorst-Pack scheme with a (3×2×1) mesh for optimization and a (3×2×1) mesh for calculations of electronic structure.

The alkaline HER reaction could be divided into two elementary reactions:

$H_2O + e- + * = *H + OH*$

$H = * + 1/2\ H_2$

Where *H signifies the H moiety on the adsorption site. The energy of H+/e- is approximately equal to the energy of 1/2 H_2.

The OER process is divide into the four fundamental reactions as following:

（1） $H_2O + * = OH* + H+ + e-$

（2） $OH* = O* + H+ + e-$

（3） $O* + H_2O = OOH* + H+ + e-$

（4） $OOH* = O_2 + H+ + e-$

OOH*, O* and OH* present the OOH, O and OH moieties on the adsorption site.

The change in Gibbs free energy (ΔG) of each adsorbed intermediate was calculated according to the computational hydrogen electrode method developed by Nørskov et al[6]. At standard conditions (T = 298.15 K, pH = 0, and U = 0 V (vs. SHE), the free energy is defined as the following equation:

$\Delta G = \Delta E + \Delta EZPE - T\Delta S$

Where ΔE represents the energy change obtained from DFT calculation, ΔEZPE is the difference between the adsorbed state and gas, which is calculated by summing vibrational frequency for all model based on the equation: $EZPE = 1/2\sum hV_i$. T is the temperature (298.15 K) in the above reaction system, and ΔS represents the difference on the entropies between the adsorbed state and gas phase. The entropies of free molecules were obtained from NIST database (https://janaf.nist.gov/). And the free energy of the adsorbed state *H can be taken as: $\Delta G^*H = \Delta E^*H + 0.24$.[7]

Reference:

[1] G. Kresse, J. Furthmüller, Comput. *Mater. Sci*. **1996**, 6, 15-50.

[2] G. Kresse, J. Furthmüller, *Phys. Rev. B* **1996**, 54, 11169-11186.

[3] M. Ernzerhof, J. P. Perdew, *J. Chem. Phys.* **1998**, 109, 3313.

[4] P. E. Blöchl, *Phys. Rev. B* **1994**, 50, 17953-17979.

[5] S. Grimme, J. Antony, S. Ehrlich, H. Krieg, *J. Chem. Phys*. **2010**, 132, 154104154119.

[6] J. K. Nørskov, J. Rossmeisl, A. Logadottir, L. Lindqvist, J. R. Kitchin, T. Bligaard, and H. Jónsson, *J. Phys. Chem. B* **2004**, 108, 46, 17886-17892

[7] J. K. Nørskov, T. Bligaard, A. Logadottir, J. R. Kitchin, J. G. Chen, S. Pandelov and U. Stimming, *J. Electrochem. Soc.* **2005**, 152, J23.

[8] J. K. Norskov, F. Abild-Pedersen, F. Studt, T. Bligaard, *Proc. Natl. Acad. Sci.* **2011**, 108, 3, 937-943.

1.2 Materials and Reagents

Ruthenium chloride ($RuCl_3$) and iridium chloride ($IrCl_3$) were purchased from Aladdin Reagents Ltd. Ammonium fluoride, Urea and ethanol were obtained from Sinopharm Chemical Reagent Co., Ltd. Nafion solution (5%), Commercial Pt/C and Commercial RuO_2 catalyst were obtained from Sigma-Aldrich Chemical Reagent Co., Ltd. All regents were analytical reagents and used without further purification.

1.3 Materials Syntheses

Firstly, 0.2 g of urea and 0.1 g of ammonium fluoride were added to 40 ml of water and 20 ml of ethanol solution until completely dissolved, followed by the addition of 2 mmol $RuCl_3$ and 0.06 mmol $IrCl_3$ and stirring until completely dissolved, then the above solutions were transferred to a 100 ml Teflon-lined autoclave and maintained at 160 ℃ for 10 h, and the sample obtained were centrifuged and dried to obtain the

precursor. The obtained precursor was then subjected to heat treatment in at different conditions (650 ℃, 4 h; 750℃, 4 h; 850℃, 4h; 950℃, 4 h) to obtain the final catalysts, which were named Ir_{SA}/RuO_2-650, Ir_{SA}/RuO_2-750, Ir_{SA}/RuO_2-850, and Ir_{SA}/RuO_2-950, respectively.

Synthesis of RuO_2: The precursor is obtained in the same way as described above except that $IrCl_3$ was not added, the synthesized samples were centrifuged as well as dried in vacuum. Subsequently, the precursor was heat-treated under 850℃, 4 h to obtain the final catalysts.

1.4 Characterization

The characterization of the synthesized products was carried out using various techniques. X-ray diffraction (XRD) was performed using a Bruker D8 diffractometer with Cu Kα radiation to investigate the crystalline structure of the products in the range of 10-80° at room temperature. Transmission electron microscopy (TEM) was used to observe the morphology and microstructure of the products. The morphology and structure were characterized by double spherical aberration-corrected scanning transmission electron microscope (AC-STEM, Titan Cubed Themis G2 300) X-ray photoelectron spectroscopy (XPS) was used to detect the surface chemical composition and state of the products. The binding energies were calibrated relative to the C1 s peak at 284.6 eV. Inductively coupled plasma optical emission spectrometer (ICP-OES) was used to detect the amount of dissolved metal in the post-reaction electrolyte. These analytical techniques were chosen to provide comprehensive information about the synthesized products, including their crystal structure, morphology, microstructure, chemical composition, and metal dissolution behavior.

1.5 Electrochemical measurements

To evaluate the electrocatalytic performance of the catalysts, a typical three-electrode cell was used, which was connected to an electrochemical workstation (CHI660E). The working electrode, reference electrode, and counter electrode were chosen as glassy carbon (GC) electrode, Hg/HgO (SCE) and graphite rod, respectively. The electrolyte is 1 mole per liter potassium hydroxide (1M/L KOH). To prepare the catalyst ink, 5 mg of the as-prepared sample and 1 mg of conductive XC-72 powder were dispersed into a mixture containing 870 μL isopropyl alcohol, 100 μL water, and 30 μL 5% Nafion solution. The mixture was then ultrasonically dispersed for 30 minutes. Afterward, 6 μL of the ink was coated on the GC electrode with a diameter of 3 mm and dried under an infrared lamp to obtain the catalyst layer with a loading of 0.425 mg cm^{-2}. For comparison, 5 mg of commercial catalyst powder (20 wt% $Pt/C/RuO_2$) was evenly dispersed into the same mixture. The ink is applied to the GC electrode for overall water splitting.

To test the performance of the catalysts for hydrogen evolution reaction (HER), linear

sweep voltammetry (LSV) was conducted with a scan rate of 5 mV s^{-1} in different potential ranges. All polarization curves were 90% iR-corrected. Electrochemical impedance spectroscopy (EIS) was performed at the corresponding potentials of 10 mA cm^{-2} obtained from the LSV curves, with a frequency range of 0.1 to 100,000 Hz. The double-layer capacitance (C_{dl}) was determined by recording cyclic voltammetry curves in the non-reactive region with a scan rate of 20 to 120 mV s^{-1}. The C_{dl} was calculated using the formula $C_{dl} = \Delta J/2v$, where ΔJ represents the current density difference and v represents the scan rate. The electrochemical specific surface area (ECSA) was calculated using the formula $ECSA = C_{dl}/C_s$, where Cs is the specific capacitance for an ideal flat surface with a real surface area of 1 cm^2. In this study, a general value of 60 μF cm^{-2} was adopted for C_s. Stability can be assessed using CV accelerating tests and chronoamperometry tests.

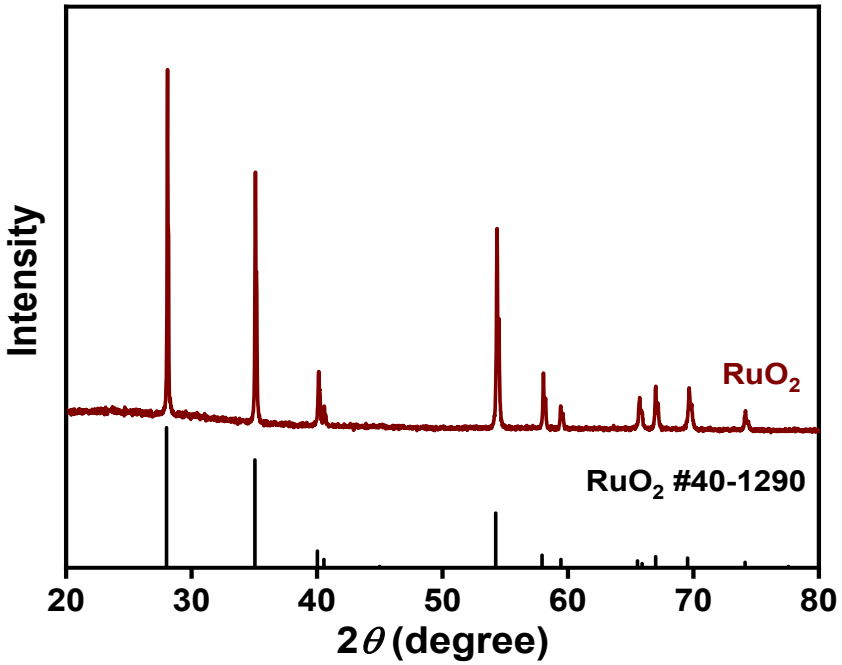

Figure S1. XRD pattern of pure RuO2.

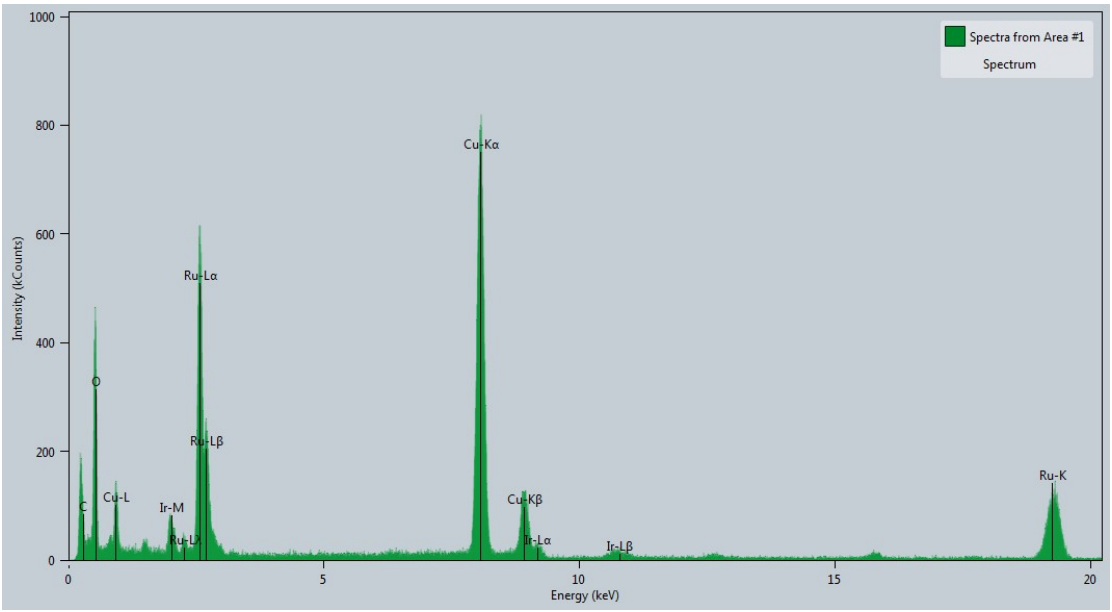

Figure S2. EDS spectrum of Ir_{SA}/RuO_2-850.

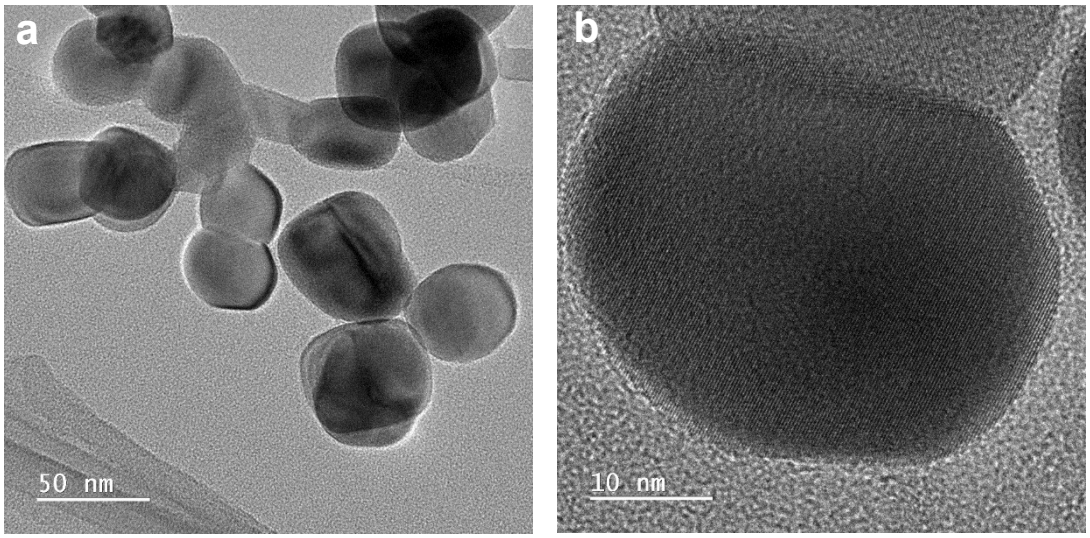

Figure S3. TEM imagines of pure RuO_2.

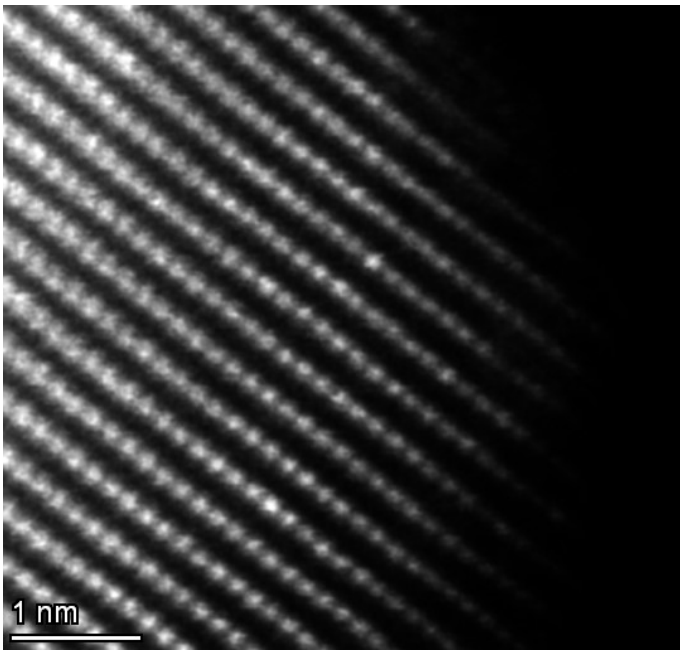

Figure S4. AC HAADF-STEM image of Ir_{SA}/RuO_2-850.

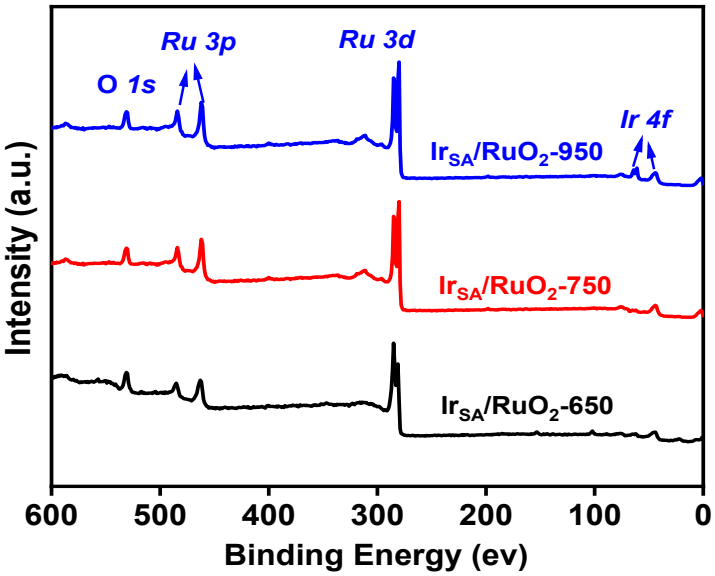

Figure S5. XPS spectrum of Ir single atom doped RuO_2.

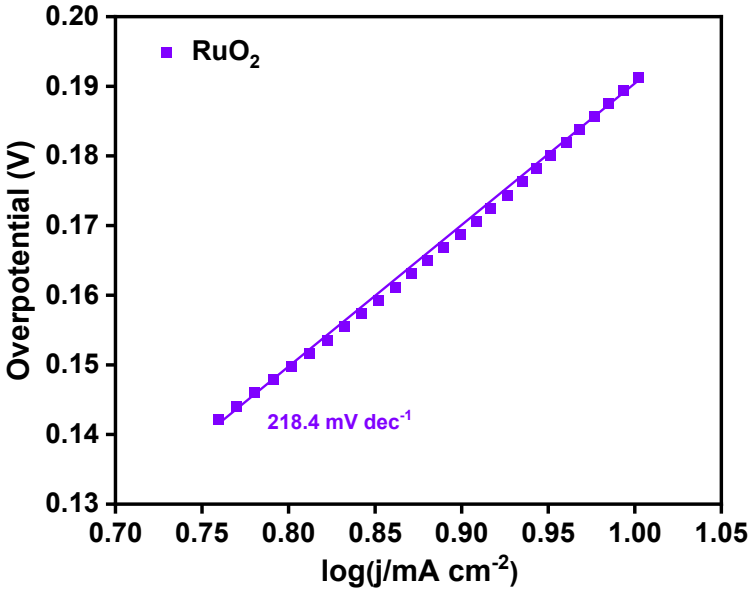

Figure S6. Tafel slopes of RuO_2.

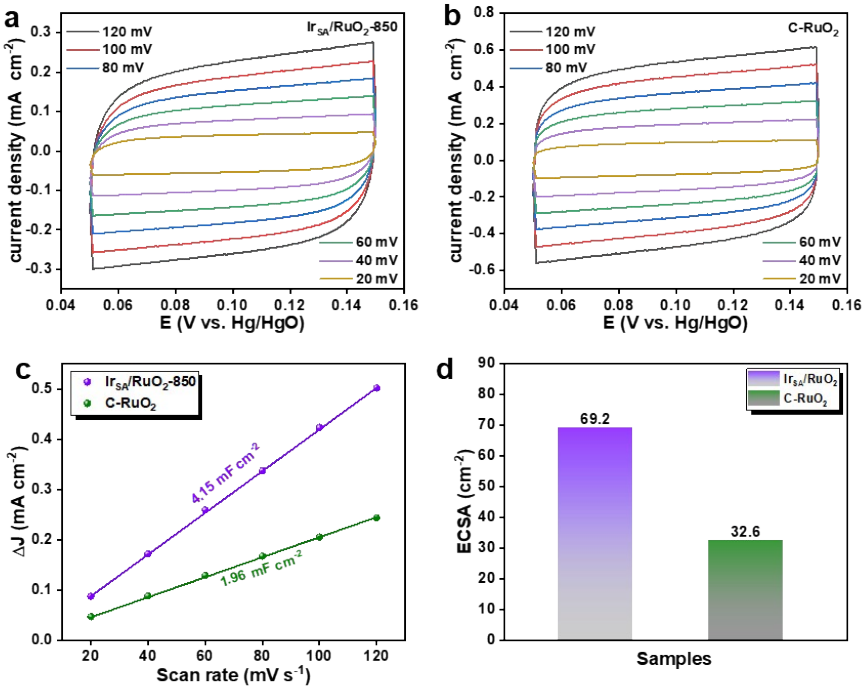

Figure S7. (a) Ir_{SA}/RuO_2-850 and (b) RuO_2 at different scan rates outside the OER region; (c) C_{dl} and (d) ECSA of Ir_{SA}/RuO_2-850 and C-RuO_2.

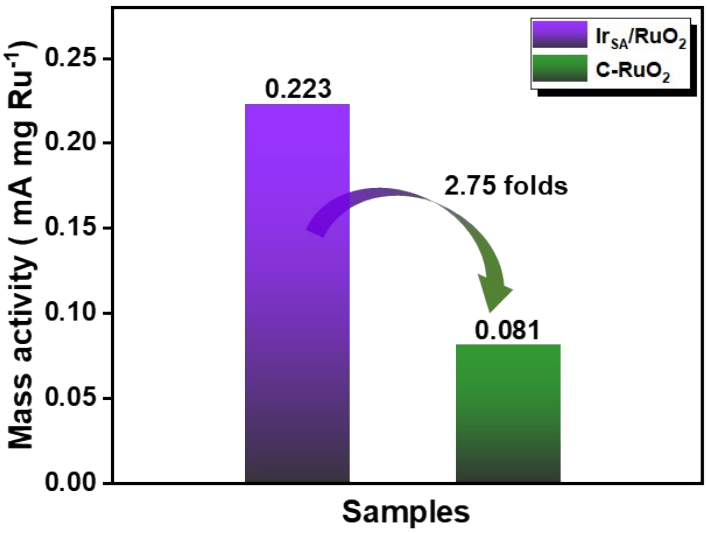

Figure S8. Mass activity of Ir_{SA}/RuO_2-850 and C-RuO_2 at overpotential of 400 mV.

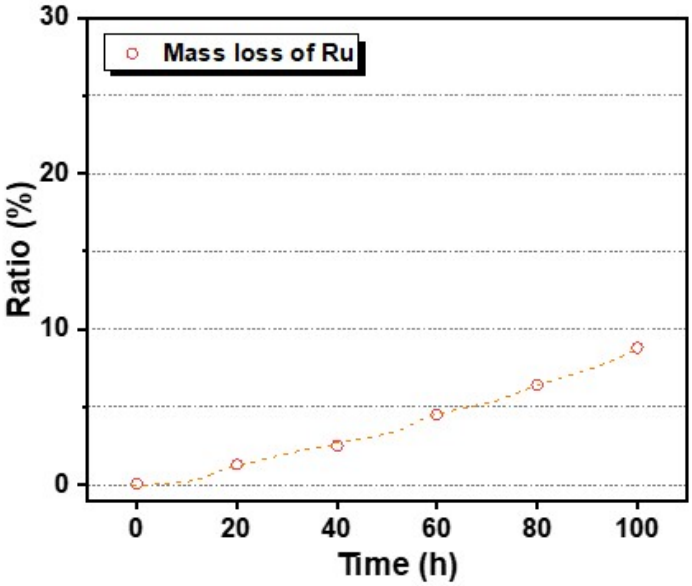

Figure S9. The dissolved amount of Ru for Ir_{SA}/RuO_2-850 during the OER stability test.

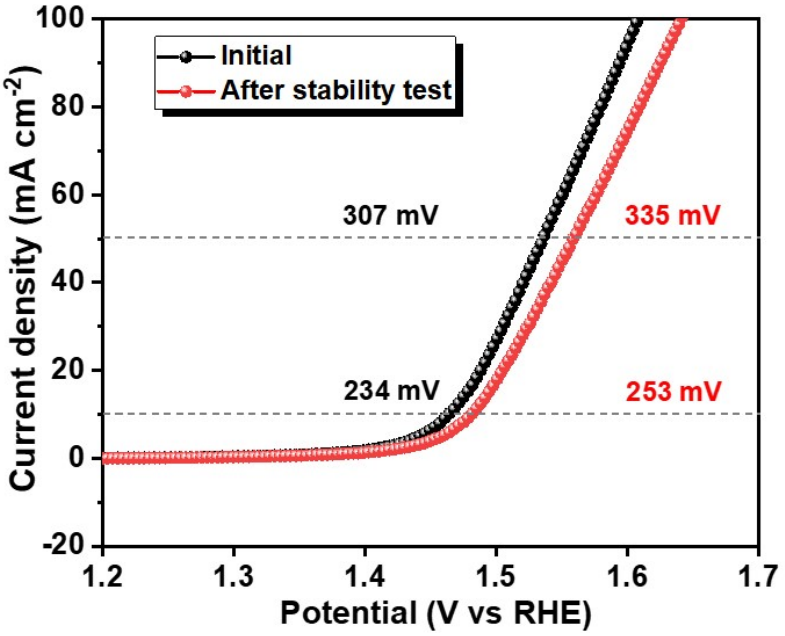

Figure S10. LSV curves of initial and after stability performance testing of Ir_{SA}/RuO_2-850 catalyst.

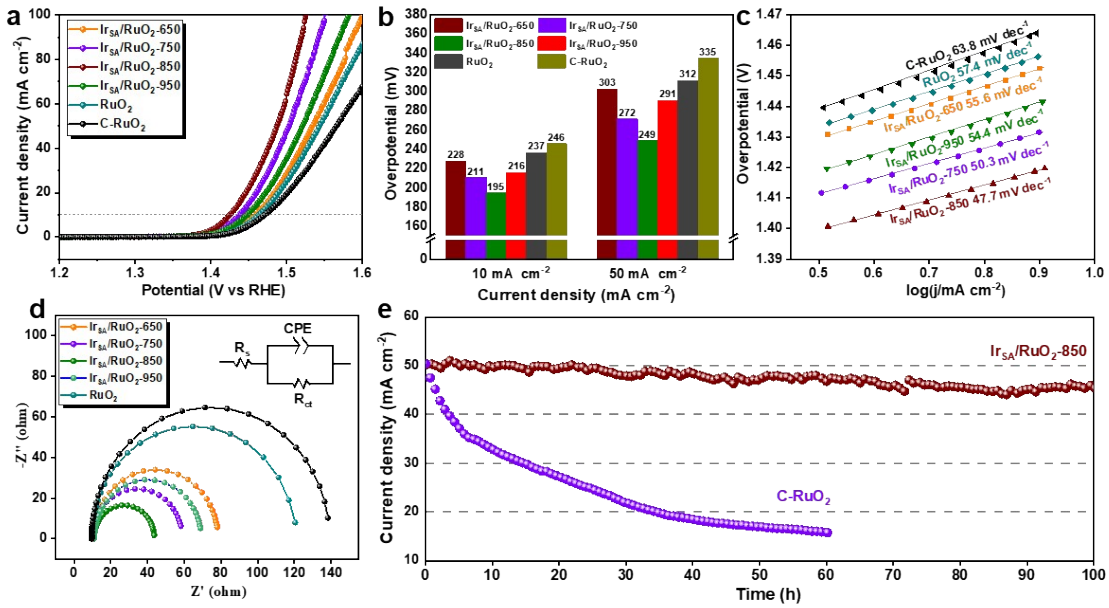

Figure S11. (a) LSV curves of OER of catalyst and (b) overpotentials at current density at 10 mA cm^{-2}, 50 mA cm^{-2} of catalysts in acidic medium; (c) Tafel slop and (d) fitted EIS curves of catalysts; (e) Chronoamperometry test curves of Ir_{SA}/RuO_2-850 and C-RuO_2.

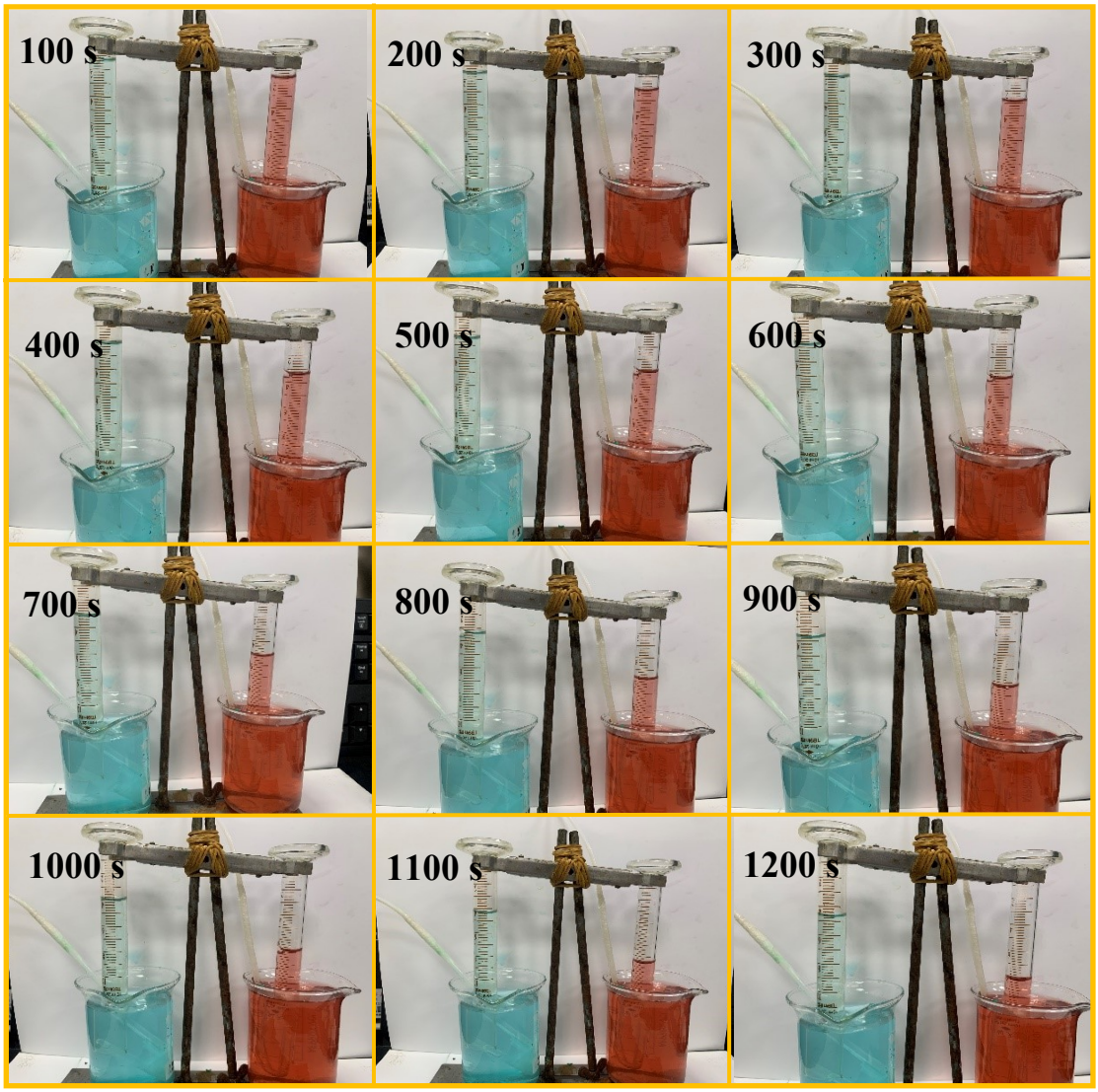

Figure S12. Digital photographs of collected H_2 and O_2 at different time.

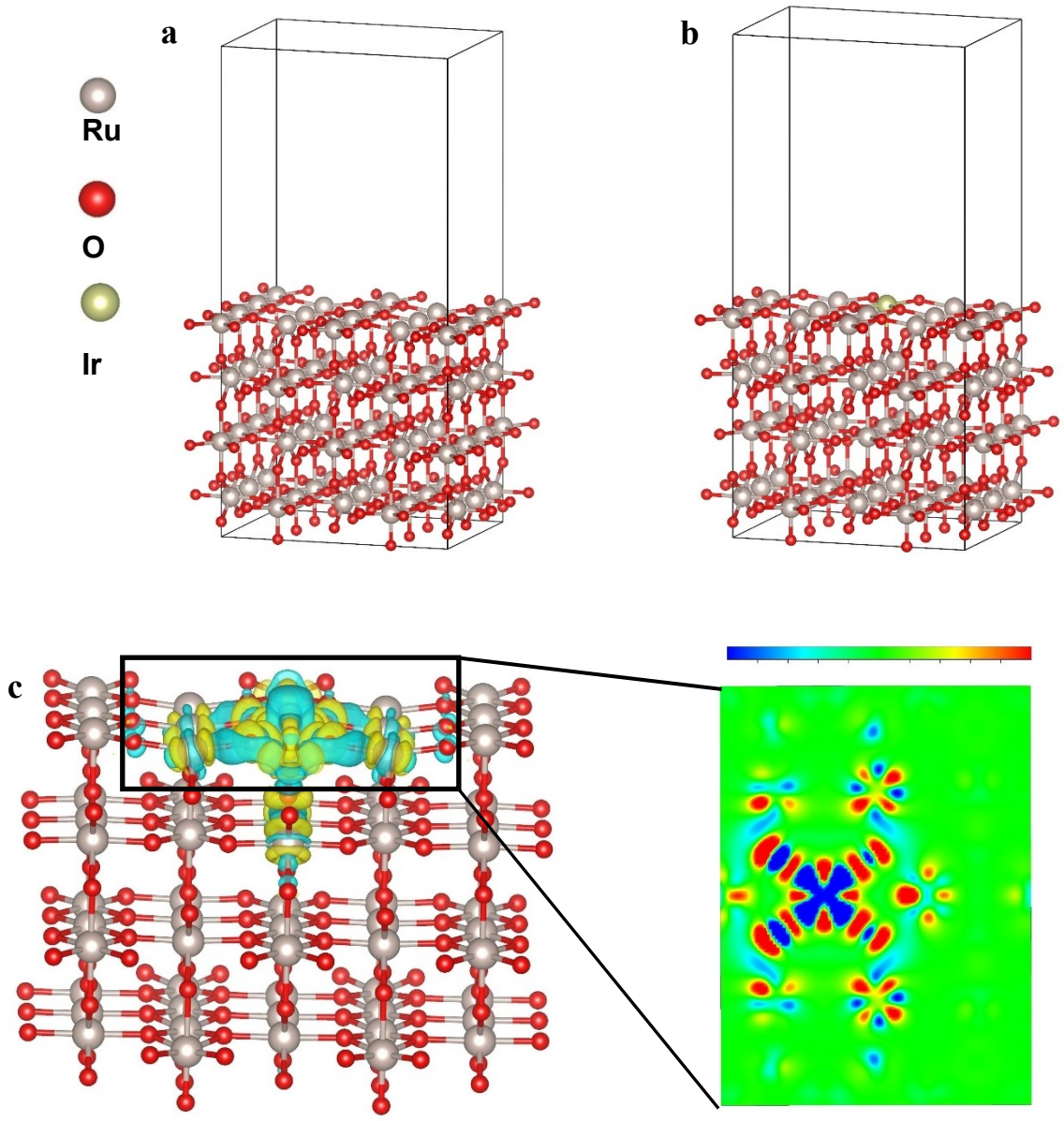

Figure S13. Optimal crystal structures of (a) RuO_2 and (b) Ir_{SA}/RuO_2, (c) charge density difference of two-dimensional slice on Ir_{SA}/RuO_2 model.

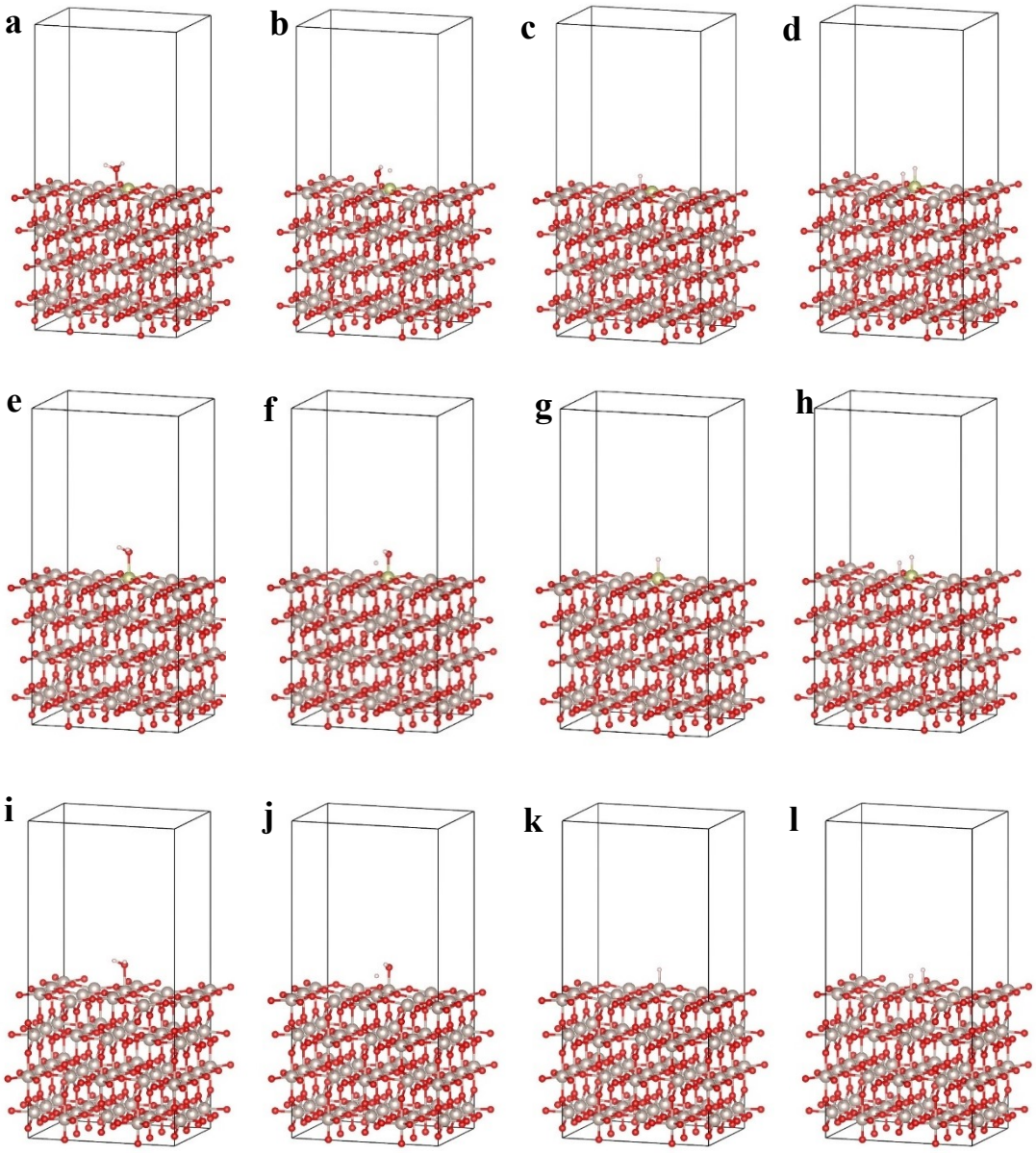

Figure S14. Adsorption configurations of reaction intermediates at various sites for HER. (a-d) H_2O, OH-H, H and 2H adsorption configurations on Ru site of Ir_{SA}/RuO_2. (e-h) H_2O, OH-H, H and 2H adsorption configurations on Ir site of Ir_{SA}/RuO_2. (i-l) H_2O, OH-H, H and 2H adsorption configurations on Ru site of RuO_2.

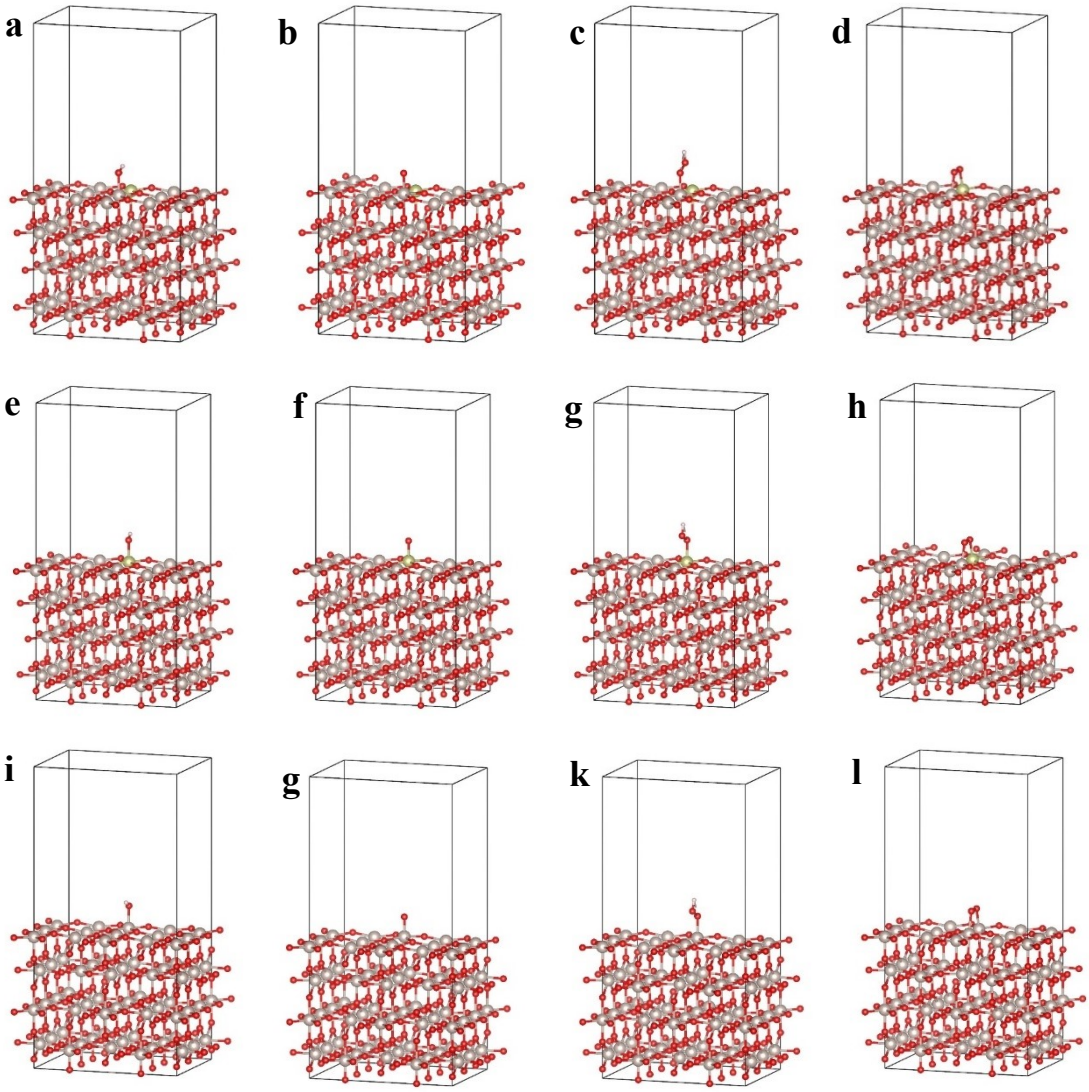

Figure S15. Adsorption configurations of reaction intermediates at various sites for HER. (a-d) OH, O, OOH and 2-O adsorption configurations on Ru site of Ir_{SA}/RuO_2. (e-h) OH, O, OOH and 2-O adsorption configurations on Ir site of Ir_{SA}/RuO_2. (i-l) OH, O, OOH and 2-O adsorption configurations on Ru site of RuO_2.

Table S1. Comparison of OER activity of Ir_{SA}/RuO_2-850 with other reported Ru-based OER electrocatalysts in alkaline media.

Catalysts	Electrolytes	η@j (mV @ mA cm^{-2})	Tafel slope (mV dec^{-1})	Reference
Ir_{SA}/RuO_2-850	1 M KOH	234@10	67.5	This work
Ru/RuO_2-PRS	1M KOH	288@10	68.67	1
Ru/RuO_2 NF	1M KOH	237.4@10	78.98	2
D-RuO_2/TiO_2/TM	1M KOH	295@10	46.6	3
RuO_2/CeO_2	1M KOH	350@10	74	4
NP-RuO_2–450	1M KOH	250@10	52.6	5
CoO_x–RuO_2/NF	1M KOH	260@50	69.6	6
$Ru/ZnRuO_2$	1M KOH	221@10	57.6	7
$Mn_{0.1}Ru_{0.9}O_2$	1M KOH	231@10	62.06	8
$Mn_{0.05}Ru_{0.95}O_2$ NFs	1M KOH	236@10	56.4	9
Mn-RuO_2	1M KOH	220@10	59.7	10
Ru@V-RuO_2/C	1M KOH	201@10	44.8	11
Ru/RuO_2-2.5 h	1M KOH	253@10	80.15	12
RuO_2-Ru/MoO_2/CC	1M KOH	231@10	58.3	13
Ru-RuO_2/C 250NA	1M KOH	273.42@10	/	14
Ru/RuO_2-MoO_2-500	1M KOH	260@10	65	15
Fe_3O_4/RuO_2-C	1M KOH	268@20	55	16
CoO_x/RuO_2@500	1M KOH	230@10	50	17
IW-Co_3O_4-RuO_2-HS	1M KOH	250@10	55.4	18
RuO_2-Co_3O_4	1M KOH	260@10	73	19

Table S2. Comparison of OER activity of Ir_{SA}/RuO_2-850 with other reported RuO_2-based OER electrocatalysts in acidic media.

Catalysts	Electrolytes	η@j (mV @ mA cm^{-2})	Tafel slope (mV dec^{-1})	Reference
Ir_{SA}/RuO_2-850	0.5 M H_2SO_4	195@10	47.7	This work
Pt-doped RuO_2	0.5 M H_2SO_4	228@10	51	20
Co-doped RuO_2	0.5 M H_2SO_4	200@10	58.2	21
Zn-doped RuO_2	0.5 M H_2SO_4	206@10	49	22
Mg-doped RuO_2	0.5 M H_2SO_4	228@10	48.6	23
Re-doped RuO_2	0.1 M $HClO_4$	190@10	45.5	24
Cu-doped RuO_2	0.5 M H_2SO_4	188@10	43.96	25
Cr-doped RuO_2	0.5 M H_2SO_4	178@10	58	26
Ce-doped RuO_2	0.5 M H_2SO_4	191@10	59.1	27
Nd-doped RuO_2	0.5 M H_2SO_4	211@10	50	28
Bi-doped RuO_2	0.5 M H_2SO_4	200@10	59.6	29
Nb-doped RuO_2	0.5 M H_2SO_4	207@10	50	30
La-doped RuO_2	0.5 M H_2SO_4	208@10	57.4	31
S-doped RuO_2	0.5 M H_2SO_4	219@10	46.1	32
S-doped RuO_2	0.5 M H_2SO_4	231@10	39.7	33
B-doped RuO_2	0.5 M H_2SO_4	200@10	55	34
Si-doped RuO_2	0.5 M H_2SO_4	220@10	53	35
Se-doped RuO_2	0.5 M H_2SO_4	190@10	43.7	36
Sr/Ir-doped RuO_2	0.5 M H_2SO_4	190@10	39	37
Mn/Fe-doped RuO_2	0.5 M H_2SO_4	270@10	41	38
Pt/Co-doped RuO_2	0.1 M $HClO_4$	213@10	48.5	39
Ni/Co-doped RuO_2	0.1 M $HClO_4$	280@10	32	40

Reference:

1 J. Hu, Y.Fu, P.Yang, L.Guo, S.Ye, X.Ren, C.He, Q.Zhang and J.Liu, *Mater. Charact.* 2021,177, 111201.

2 Y. Hou, Z. Qin, X. Han, Y. Liu, W. Zhang, X. Cao, Y. Cao, J.-P. Lang and H. Gu, *Nanoscale*, 2024, **16**, 6662–6668.

3 W. Li, H. Zhang, M. Hong, L. Zhang, X. Feng, M. Shi, W. Hu and S. Mu, *Chem. Eng. J.*, 2022, **431**, 134072.

4 S. M. Galani, A. Mondal. D. N. Srivastava and A. B. Panda. *Int. J. Hydrogen Energy, 2020, 45, 18635-18644*.

5 N. Cong, Y. Han, C. Zhai, H. Chen, J. Han, H. Fang, X. Zhou, Y. Zhu, Z. Ren, *J. Electroanal. Chem., 2021, 881, 114955.*

6 T. Yu, Q. Xu, G. Qian, J. Chen, H. Zhang, L. Luo and S. Yin, *ACS Sustainable Chem. Eng.*, 2020, **8**, 17520–17526.

7 X. Zhang, Z. Su, D. Xiang, W. Xu, Q. Guo, Y. Fan, X. Kang, Y. Sheng, F. Zheng and W. Chen, *Adv. Funct. Mater.*, 2024, 2409306.

8 X. Dong, Y. Wang, J. Wang, Y. Sun, B. Xu, C. Li and L. Hang, *International Journal of Hydrogen Energy*, 2024, **73**, 558–565.

9 W. Li, R. Liu, G. Yu, X. Chen, S. Yan, S. Ren, J. Chen, W. Chen, C. Wang and X. Lu, *Small*, 2024, **20**, 2307164.

10 J. Cao, D. Zhang, B. Ren, P. Song and W. Xu, *Chin. Chem. Lett. 2024, 35, 109863*.

11 Y. Li, W. Wang, M. Cheng, Y. Feng, X. Han, Q. Qian, Y. Zhu and G. Zhang, *Adv. Mater.*, 2023, **35**, 2206351.

12 S. L. D. Nicole, Y. Li, W. Xie, G. Wang and J. Lee, *Small*, 2023, **19**, 2206844.

13 J.-L. Cai, J.-Y. Fan, X.-D. Zhang, X. Xie, W.-Y. Tian, X.-G. Zhang, J. Ding and Y.-S. Liu, *Rare Met.*, DOI:10.1007/s12598-024-02772-z.

14 Y. Cong, D. Dou, L. Zhang, H. Wang, M. Liu, L. Chen, Q. Zhao and C. Li, *Fuel*, 2024, **367**, 131472.

15 Y. Fan, X. Zhang, Y. Zhang, X. Xie, J. Ding, J. Cai, B. Li, H. Lv, L.Liu, M. Zhu, X. Zhaeng, Q. Cai, Y. Liu and S. Lu., *J. Colloid Interface Sci.,* 2021, 604, 508-516.

16 A. Shekhawat, R. Samanta and S. Barman, *ACS Appl. Energy Mater*., 2022, 5, 6059-6069.

17 L. Zeng, G. Mao, Y. Zhu, R. Li, Q. Zhou, F. Xiao and R. Tang, *Applied Surface Science*.2022, 589. 152958.

18 Y. Gao, D. Zheng, Q. Li, W. Xiao, T. Ma, Y. Fu, Z. Wu and L. Wang, *Adv. Funct. Mater.*, 2022, **32**, 2203206.

19 F. Ren, J. Xu and L. Feng, *Nano Res.*, 2024, **17**, 3785–3793.

20 J. Wang, H. Yang, F. Li, L. Li, J. Wu, S. Liu, T. Cheng, Y. Xu, Q. Shao and X. Huang, *Sci. Adv.*, 2022, **8**, l9271.

21 J. Shan, T. Ling, K. Davey, Y. Zheng and S. Qiao, *Adv. Mater.*, 2019, **31**, 1900510.

22 H. Zhang, B. Wu, J. Su, K. Zhao and L. Chen, *ChemNanoMat*, 2021, **7**, 117–121.

23 Z. Li, S. Wang, Y. Tian, B. Li, H. J. Yan, S. Zhang, Z. Liu, Q. Zhang, Y. Lin and L. Chen, *Chem. Commun.*, 2020, **56**, 1749–1752.

24 H. Jin, X. Liu, P. An, C. Tang, H. Yu, Q. Zhang, H.-J. Peng, L. Gu, Y. Zheng, T. Song, K. Davey, U. Paik, J. Dong and S.-Z. Qiao, *Nat. Commun.*, 2023, **14**, 354.

25 J. Su, R. Ge, K. Jiang, Y. Dong, F. Hao, Z. Tian, G. Chen and L. Chen, *Adv. Mater.*, 2018, **30**, 1801351.

26 Y. Lin, Z. Tian, L. Zhang, J. Ma, Z. Jiang, B. J. Deibert, R. Ge and L. Chen, *Nat. Commun.*, 2019, **10**, 162.
27 J. Bai, L. Cheng, S. Liu, H. Zhang, Y. Lian, Y. Deng, Q. Zhou, Y. Tang and Y. Su, *Appl. Surf. Sci.*, 2024, **642**, 158613.
28 L. Li, G. Zhang, J. Xu, H. He, B. Wang, Z. Yang and S. Yang, *Adv. Funct. Mater.,* 2023, 33, 2213304.
29 L. Wu, Q. Liang, J. Zhao, J. Zhu, H. Jia, W. Zhang, P. Cai and W. Luo, *Chin. J. Catal.*, 2023, **55**, 182–190.
30 H. Liu, Z. Zhang, J. Fang, M. Li, M. G. Sendeku, X. Wang, H. Wu, Y. Li, J. Ge, Z. Zhuang, D. Zhou, Y. Kuang and X. Sun, *Joule*, 2023, **7**, 558–573.
31 Y. Wu, R. Yao, Q. Zhao, J. Li and G. Liu, *Chem. Eng. J.*, 2022, **439**, 135699.
32 L. Liu, Y. Ji, W. You, S. Liu, Q. Shao, Q. Kong, Z. Hu, H. Tao, L. Bu and X. Huang, *Small*, 2023, **19**, 2208202.
33 Q. Yao, Z. Yu, Y.-H. Chu, Y.-H. Lai, T.-S. Chan, Y. Xu, Q. Shao and X. Huang, *Nano Res.*, 2022, **15**, 3964–3970.
34 C. Liu, B. Sheng, Q. Zhou, D. Cao, H. Ding, S. Chen, P. Zhang, Y. Xia, X. Wu and L. Song, *Nano Res.*, 2022, **15**, 7008–7015.
35 C. Liu, Y. Jiang, T. Wang, Q. Li and Y. Liu, *Adv. Sci.*, 2023, **10**, 2207429.
36 K. Huang, C. Lin, G. Yu, P. Du, X. Xie, X. He, Z. Zheng, N. Sun, H. Tang, X. Li, M. Lei and H. Wu, *Adv. Funct. Mater.*, 2023, **33**, 2211102.
37 Y. Wen, P. Chen, L. Wang, S. Li, Z. Wang, J. Abed, X. Mao, Y. Min, C. T. Dinh, P. D. Luna, R. Huang, L. Zhang, L. Wang, L. Wang, R. J. Nielsen, H. Li, T. Zhuang, C. Ke, O. Voznyy, Y. Hu, Y. Li, W. A. Goddard Iii, B. Zhang, H. Peng and E. H. Sargent, *J. Am. Chem. Soc.*, 2021, **143**, 6482–6490.
38 Z. Fan, J. Jiang, L. Ai, Z. Shao and S. Liu, *ACS Appl. Mater. Interfaces*, 2019, **11**, 47894–47903.
39 H. Jin, S.Choi, G. j. Bang, T. Kwon, H. S. Kim, S. J. Lee, Y. hong, D. K. Lee, H. S. Park, H. Bail, Y. Jung, S. J. Yoo and K. Lee, Energy *Environ. Sci*., 2022, 15, 1119.
40 Y. Wu, M. Tariq, W. Q. Zaman, W. Sun, Z. Zhou and J. Yang, *ACS Appl. Energy Mater.*, 2019, **2**, 4105–4110.